Linear analysis of periodic-waveguide cyclotron maser interaction

Eli Jerby

Faculty of Engineering, Tel Aviv University, Ramat Aviv 69978, Israel

Following recent experimental studies, we present in this paper a linear model of the periodic-waveguide cyclotron maser. This device is based on a cyclotron-type interaction of a nonrelativistic electron beam with traveling waves in a metallic periodic waveguide. The kinetic model presented in this paper incorporates the periodic-waveguide spatial wave harmonics with the cyclotron and Weibel interactions. It results in a Pierce-type gain-dispersion equation with new coupling terms. The dependence of the cyclotron amplification on the low impedance of the inductive periodic waveguide and on the electron initial transverse velocity is analyzed in various operating regimes. In agreement with experimental results, this analysis shows that amplification is feasible in certain conditions without an initial electron transverse velocity ($V_{0\perp} = 0$) and with a wide acceptance of electron beam energy variation.

PACS number(s): 52.75.Ms, 42.52.+x, 52.35.Hr

I. INTRODUCTION

Various types of well known *fast-wave* cyclotron maser devices [1–11] have been developed on the basis of the electron cyclotron instability [12]. A typical scheme of a fast-wave cyclotron resonance maser (CRM) consists of a relativistic electron beam which interacts with a fast electromagnetic (em) wave in a uniform waveguide. The electrons are spiraling in the CRM device by an axial magnetic field which satisfies a cyclotron resonance condition with the em wave and the electron beam. Relativistic effects play a dominant role in the CRM-type devices [5]. The azimuthal bunching is a consequence of the electron mass variation caused by the transverse electromagnetic accelerating and decelerating forces. The electrons in these devices are injected into the interaction region with an initial transverse velocity component essential for the relativistic cyclotron interaction.

The *slow-wave* cyclotron (SWC) maser, in which the em wave is slowed down by a dielectric-loaded waveguide, has been studied in various schemes [13–21]. The SWC mechanism of interaction differs from that of the fast-wave cyclotron masers though both satisfy similar cyclotron resonance conditions. The dominant bunching effect in the SWC stems from the $\mathbf{V}_\perp \times \mathbf{B}_\perp$ axial force component referred to the Weibel mechanism, whereas the dominant effect in the fast-wave cyclotron devices is the relativistic azimuthal bunching which results from the electron energy variation $\dot{\gamma}$ due to the stationary $\mathbf{V}_\perp \cdot \mathbf{E}_\perp$ product, where $\mathbf{V}_\perp$ is the electron transverse cyclotron velocity and $\mathbf{E}_\perp$ and $\mathbf{B}_\perp$ are the electric and magnetic field components of the em wave, respectively. The typical advantages of the SWC in comparison with the fast-wave cyclotron devices are a wider frequency band and a lower operating electron beam energy. The SWC, however, is more sensitive than the conventional CRM to the electron beam energy spread [16]. In addition, the presence of a dielectric material in the vicinity of an electron beam introduces technical difficulties for the dielectric-loaded SWC operation.

Cyclotron amplifier and oscillator experiments in metallic periodic waveguides have been conducted recently at M.I.T and later at Tel Aviv University [22–25]. The periodic waveguide used in these experiments consist of an array of metal posts in rectangular waveguide as shown in Fig. 1. A low-energy electron beam (~ 8 keV, ~ 1 A) interacts in this periodic waveguide with traveling waves in a frequency range of 8–10 GHz under an axial magnetic field of 3–4 kG. Clear cyclotron resonance conditions have been observed in these experiments, both in the amplifier gain curves [22,23] and in the oscillator output frequency [23–25]. Electronic gain of ~ 10 dB and rf power of ~ 400 W have been measured in the amplifier and oscillator experiments, respectively.

The similarity between the dielectric-loaded SWC maser and the periodic-waveguide cyclotron maser stems from the *artificial dielectric* properties of the periodic waveguide [26]. The theoretical analysis presented in this paper shows that their dominant mechanisms of operation are different despite their resemblance. They differ also in their typical spectral bandwidth and electron spread acceptance parameters. From the technical point of view, the use of a metallic periodic waveguide, rather than a dielectric loaded waveguide as in the SWC maser, alleviates the technical difficulties which result from the
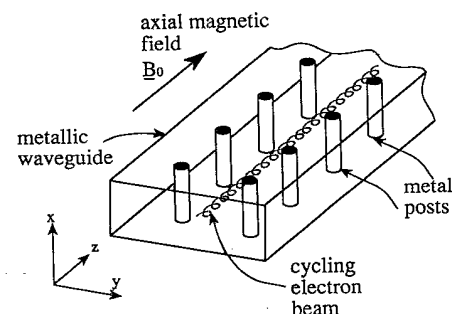

FIG. 1. A principle scheme of the periodic-waveguide cyclotron device.

<u>49</u>   4487

presence of a dielectric insulator in the vicinity of a high-power electron beam. Hence the periodic-waveguide cyclotron maser has the potential to be a practical low-voltage high-power microwave source.

In the following sections we derive a linear kinetic model for the convective cyclotron interaction in periodic waveguide and analyze its properties. The effects of the periodic waveguide impedance and the initial transverse electron velocity on the cyclotron gain are analyzed. The feasibility of amplification with zero initial transverse electron velocity component is discussed. The operating frequency bandwidth of the periodic-waveguide cyclotron and its electron spread acceptance are evaluated in comparison with the known CRM and SWC devices.

II. DERIVATION OF DISPERSION RELATION

A kinetic linear model is derived in this section for the convective cyclotron instability in periodic waveguide. We assume a tenuous electron beam spiraling along a uniform axial magnetic field. The electrons interact with traveling wave harmonics in the periodic waveguide shown in Fig. 1.

Assuming a slowly varying wave amplitude $A(z)$ along the interaction region, the em wave propagating in the periodic waveguide is described as a composition of spatial harmonics,

$$E_x(z) = A(z) \sum_n e_{xn}\phi_n(x,y)e^{-j\beta_n z}, \tag{1a}$$

$$H_y(z) = A(z) \sum_n h_{yn}\phi_n(x,y)e^{-j\beta_n z}, \tag{1b}$$

where e_{xn} and h_{yn} are the nth harmonic electric and magnetic field coefficients, respectively, and $\phi_n(x,y)$ is their transverse profile. The harmonic wave number $\beta_n(\omega)$ is determined by the waveguide dispersion relation. In this analysis we use without loss of generality the relations derived in the Appendix for the periodic waveguide employed in our experiments [22–25]. This waveguide, shown in Fig. 1, consists of an array of metal posts in a rectangular metal tube. The results of this analysis are applicable to other periodic waveguides as well (and in particular to the slotted periodic waveguide in Ref. [27]).

The wave equation for the H_y magnetic field component is given by

$$\nabla^2 H_y + \epsilon_r k^2 H_y = -\partial_z J_x + \partial_x J_z, \tag{2}$$

where ϵ_r is the relative dielectric constant of the medium ($\epsilon_r = 1$ for a metallic periodic waveguide, and > 1 for a dielectric loaded waveguide) and $k = \omega/c$ is the free space wave number. The axial current J_z is out of the cyclotron resonance and therefore the term $\partial_x J_z$ is considered negligible in this analysis. The dominant current component J_x is computed in the linear regime by

$$J_x = -\frac{e}{m_0} \int\int\int_{\mathbf{P_0}} \frac{P_{cx}}{\gamma_0} f_{1c}(\mathbf{P_0},z,\omega)\, d^3P_0, \tag{3}$$

where P_{cx} is the $\hat{\mathbf{x}}$ component of the characteristic line $\mathbf{P_c}(\mathbf{P_0})$ of the zero-order Vlasov equation, $f_{1c}(\mathbf{P_0},z,\omega)$ is the electron first-order distribution function, and e and m_0 are the electron charge and rest mass, respectively. The characteristic line describes the momentum of a single electron spiraling along the axial magnetic field $\mathbf{B_0} = \hat{\mathbf{z}}B_{0z}$ and is given by

$$\mathbf{P_c} = \hat{\mathbf{x}}P_{0\perp}\cos(k_c z + \alpha_0) + \hat{\mathbf{y}}P_{0\perp}\sin(k_c z + \alpha_0) + \hat{\mathbf{z}}P_{0z}. \tag{4}$$

The initial values of the characteristic line are given in cylindrical coordinates by the initial axial and radial electron velocity components, P_{0z} and $P_{0\perp}$, respectively, and by α_0, the initial phase of the electron gyromotion. These are related to the Cartesian (P_{0x}, P_{0y}, P_{0z}) initial momentum components by

$$P_{0\perp} = \sqrt{P_{0x}^2 + P_{0y}^2}, \tag{5a}$$

$$\alpha_0 = \tan^{-1}\frac{P_{0y}}{P_{0x}}. \tag{5b}$$

Both Cartesian and cylindrical coordinate systems are used simultaneously in the following analysis.

The relativistic factor in Eq. (3) is given by

$$\gamma_0 = \sqrt{1 + (P_{0z}^2 + P_{0\perp}^2)/m_0^2 c^2}. \tag{6}$$

It should be emphasized that relativistic effects must be taken into account in this analysis as in the cyclotron resonance maser analysis [5] even though the interaction may occur with a low energy ($\gamma_0 \sim 1$) electron beam (note that the electron energies in our recent experiments [22–25] are less than 10 keV).

The cyclotron wave number in Eq. (4) is given by $k_c = \omega_c/V_{0z}$ where $V_{0z} = P_{0z}/\gamma_0 m_0$ is the axial velocity component of the electron. The relativistic cyclotron frequency ω_c is given by

$$\omega_c = \frac{\omega_{c0}}{\gamma_0}, \tag{7}$$

where $\omega_{c0} = eB_{0z}/m_0$ is the nonrelativistic cyclotron frequency.

The first-order distribution function $f_{1c}(\mathbf{P_0},z,\omega)$ in Eq. (3) is the solution of the first-order Vlasov equation integrated along the zero-order characteristic lines (4) as follows:

$$j\bar{\omega}f_{1c}(\mathbf{P_0},z,\omega) + \frac{P_{cz}}{\gamma_0 m_0}\frac{\partial}{\partial z}f_{1c} + \mathbf{F_{1c}}\cdot\nabla_{\mathbf{p_0}}f_{0c}(\mathbf{P_0}) = 0, \tag{8}$$

where $f_{0c}(\mathbf{P_0})$ is the electron zero-order distribution function at the entrance ($z = 0$) to the interaction region. The first-order force induced by the transverse fields (1a) and (1b) along the characteristics in the periodic waveguide is given by

$$\mathbf{F_{1c}} = -e\left[\hat{\mathbf{x}}\left(E_x - \frac{P_{cz}}{\gamma_0 m_0}\mu_0 H_y\right) + \hat{\mathbf{z}}\frac{P_{cx}}{\gamma_0 m_0}\mu_0 H_y\right]. \tag{9}$$

Assuming a uniform initial azimuthal distribution of the electron beam, the function $f_{0c}(\mathbf{P_0})$ is independent of α_0. Consequently, $\partial f_{0c}/\partial P_{0x} = (P_{0x}/P_{0\perp})\partial f_{0c}/\partial P_{0\perp}$, and the Vlasov equation (8) is rewritten in the form

$$j\omega f_{1c}(P_{0\perp}, P_{0z}, z, \omega) + \frac{P_{0z}}{\gamma_0 m_0}\frac{\partial}{\partial z}f_{1c}$$

$$= e\left(E_x - \frac{P_{0z}}{\gamma_0 m_0}\mu_0 H_y\right)\cos(k_c z + \alpha_0)\frac{\partial f_{0c}}{\partial P_{0\perp}}$$

$$+ e\frac{P_{0\perp}}{\gamma_0 m_0}\cos(k_c z + \alpha_0)\mu_0 H_y\frac{\partial f_{0c}}{\partial P_{0z}}. \qquad (10)$$

Equations (2), (3), and (10) form a linear set of partial differential equations. In order to solve them, we apply Laplace transform on the z dimension,

$$\tilde{A}(s) = \int_z A(z)e^{-sz}dz, \qquad (11)$$

and rewrite Eqs. (2), (3), and (10) in the s domain as follows. The wave equation (2) is transformed to

$$\left(\frac{\partial^2}{\partial y^2} + s^2 + \epsilon_r k^2\right)\tilde{H}_y(s,\omega) - (s + \partial_z)H_y(\omega, z = 0)$$

$$= -s\tilde{J}_x(s,\omega), \qquad (12)$$

where the current $\tilde{J}_x(s,\omega)$ is given in s plane by a Laplace transform of Eq. (3) in the form

$$\tilde{J}_x(s,\omega) = -\frac{e}{2m_0}\int\int\int_{\mathbf{P_0}}\frac{P_{0\perp}}{\gamma_0}[e^{j\alpha_0}\tilde{f}_{1c}(s - jk_c)$$

$$+ e^{-j\alpha_0}\tilde{f}_{1c}(s + jk_c)]d^3P_0. \qquad (13)$$

The first-order distribution function $\tilde{f}_{1c}$ is given by the solution of the transformed first-order Vlasov equation (10) as follows:

$$\tilde{f}_{1c}(P_{0\perp}, P_{0z}, s, \omega) = \frac{e}{2}\left[j\omega + \frac{P_{0z}}{\gamma_0 m_0}s\right]^{-1}\left\{\left[e^{j\alpha_0}\left(\tilde{E}_x(s - jk_c) - \frac{P_{0z}}{\gamma_0 m_0}\mu_0\tilde{H}_y(s - jk_c)\right)\right.\right.$$

$$+ e^{-j\alpha_0}\left(\tilde{E}_x(s + jk_c) - \frac{P_{0z}}{\gamma_0 m_0}\mu_0\tilde{H}_y(s + jk_c)\right)\left]\frac{\partial f_{0c}}{\partial P_{0\perp}}\right.$$

$$+ \frac{\mu_0 P_{0\perp}}{\gamma_0 m_0}\left[e^{j\alpha_0}\tilde{H}_y(s - jk_c) + e^{-j\alpha_0}\tilde{H}_y(s + jk_c)\right]\frac{\partial f_{0c}}{\partial P_{0z}}\bigg\}. \qquad (14)$$

Substituting the distribution function (14) into the current integral (13) results in the expression

$$\tilde{J}_x(s,\omega) \cong -\frac{\pi e^2}{2m_0}\int_{P_{0\perp}}\int_{P_{0z}}\frac{P_{0\perp}}{\gamma_0}\left[j\omega + \frac{P_{0z}}{\gamma_0 m_0}s - \frac{j\omega_{c0}}{\gamma_0}\right]^{-1}$$

$$\times\left\{\left[\tilde{E}_x(s) - \frac{P_{0z}}{\gamma_0 m_0}\mu_0\tilde{H}_y(s)\right]\frac{\partial f_{0c}}{\partial P_{0\perp}} + \frac{P_{0\perp}}{\gamma_0 m_0}\mu_0\tilde{H}_y(s)\frac{\partial f_{0c}}{\partial P_{0z}}\right\}P_{0\perp}dP_{0\perp}dP_{0z}, \qquad (15)$$

where we assume that the dominant poles are located in s plane in the vicinity of the cyclotron resonance condition

$$\left|j\omega + \frac{P_{0z}}{\gamma_0 m_0}s - \frac{j\omega_{c0}}{\gamma_0}\right| \sim 0, \qquad (16)$$

and that the cyclotron sideband harmonics, $\tilde{E}_x(s \pm j2k_c)$ and $\tilde{H}_y(s \pm j2k_c)$, are negligible. After an integration by parts and some further algebraic steps, Eq. (15) results in

$$\tilde{J}_x(s,\omega) = \frac{\pi e^2}{m_0}\int_{P_{0\perp}}\int_{P_{0z}}\frac{1}{\gamma_0}\left\{\left(j\omega + \frac{P_{0z}}{\gamma_0 m_0}s - j\omega_{c0}/\gamma_0\right)^{-1}\left[\tilde{E}_x(s) - \frac{P_{0z}}{\gamma_0 m_0}\mu_0\tilde{H}_y(s)\right]\right.$$

$$\left.- \frac{P_{0\perp}^2}{2\gamma_0^2 m_0^2}\left(j\omega + \frac{P_{0z}}{\gamma_0 m_0}s - j\omega_{c0}/\gamma_0\right)^{-2}\left[\frac{j\omega}{c^2}\tilde{E}_x(s) + s\mu_0\tilde{H}_y(s)\right]\right\}f_{0c}P_{0\perp}dP_{0\perp}dP_{0z}. \qquad (17)$$

In the ideal case of a cold and azimuthaly uniform electron beam, the zero-order electron distribution on-axis $f_{0c}(\mathbf{P_0})$ is approximated by

$$f_0(\mathbf{P_0}) = \frac{1}{2\pi\bar{P}_{0\perp}}\delta(P_{0\perp} - \bar{P}_{0\perp})\delta(P_{0z} - \bar{P}_{0z})n_0, \qquad (18)$$

where n_0 is the electron density. Substituting Eq. (17) in the ideal limit (18) into the wave equation (12), results in the dispersion equation

$$\left(\frac{\partial^2}{\partial y^2} + s^2 + \epsilon_r k^2\right)\tilde{H}_y(s,\omega) - (s + \partial_z)H_y(\omega, z=0)$$

$$= -\frac{1}{2}\epsilon_0\omega_{p0}^2 g_0(x,y)\frac{s}{j(\omega-\omega_c)+s\bar{V}_{0z}}\left\{\tilde{E}_x(s) - \bar{V}_{0z}\mu_0\tilde{H}_y(s) - \frac{\bar{V}_{0\perp}^2}{2}\frac{1}{j(\omega-\omega_c)+s\bar{V}_{0z}}\left[\frac{j\omega}{c^2}\tilde{E}_x(s) + s\mu_0\tilde{H}_y(s)\right]\right\}, \tag{19}$$

where $\omega_{p0} = \sqrt{e^2 n_0/\gamma_0 m_0 \epsilon_0}$ is the plasma frequency, $g_0(x,y)$ is the electron beam density profile, and $\bar{V}_{0z} = \bar{P}_{0z}/\bar{\gamma}_0 m_0$ and $\bar{V}_{0\perp} = \bar{P}_{0\perp}/\bar{\gamma}_0 m_0$ are the average electron axial and perpendicular velocity components, respectively.

In the limit of a plane em wave ($\tilde{E}_x = -j\omega\mu_0\tilde{H}_y/s$) and a transversly uniform electron beam ($g_0 = 1$), we obtain as a benchmark for Eq. (19) the known dispersion relation for the cyclotron resonance maser [2–8]

$$s^2 + \epsilon_r k^2 = \frac{1}{2}\frac{\omega_{p0}^2}{c^2}\left\{\frac{j\omega + s\bar{V}_{0z}}{j(\omega-\omega_c)+s\bar{V}_{0z}} + \frac{\bar{V}_{0\perp}^2}{2}\frac{k^2+s^2}{[j(\omega-\omega_c)+s\bar{V}_{0z}]^2}\right\}. \tag{20}$$

The factor $1/2$ in the right hand side of Eq. (20) stems from the linear polarization of the wave in our analysis. Variants of this equation are applicable in general to uniform waveguide cyclotron masers including dielectric-loaded SWC's.

In a periodic waveguide, the harmonic content of the em field components (1a) and (1b) is transformed to

$$\tilde{E}_x(s,\omega) = \sqrt{\frac{\mu_0}{\epsilon_0}}\sum_n h_{yn}\hat{Z}_n\phi_n(y)\tilde{A}(s+j\beta_n), \tag{21a}$$

$$\tilde{H}_y(s,\omega) = \sum_n h_{yn}\phi_n(y)\tilde{A}(s+j\beta_n), \tag{21b}$$

where the normalized impedance of the nth spatial harmonic is defined here as

$$\hat{Z}_n = \sqrt{\frac{\epsilon_0}{\mu_0}}\frac{e_{xn}}{h_{yn}}. \tag{21c}$$

Substituting Eqs. (21a), (21b), and (21c) into Eq. (19) results in a generalized dispersion equation,

$$\sum_n (s-j\beta_n)\left[(s+j\beta_n)\tilde{A}(s+j\beta_n) - A_0\right]h_{yn}\phi_n(y)$$

$$= -\frac{1}{2c}g_0(x,y)\omega_{p0}^2\sum_m \frac{s}{j(\omega-\omega_c)+s\bar{V}_{0z}}\left\{\hat{Z}_m - \bar{\beta}_{ez} - \frac{1}{2}\bar{\beta}_{e\perp}^2\frac{j\omega\hat{Z}_m + sc}{j(\omega-\omega_c)+s\bar{V}_{0z}}\right\}h_{ym}\phi_m(y)\tilde{A}(s+j\beta_m), \tag{22}$$

where $\bar{\beta}_{ez} = \bar{V}_{0z}/c$ and $\bar{\beta}_{e\perp} = \bar{V}_{0\perp}/c$ are the normalized electron velocity components.

In order to find the growth rate of the wave amplitude $A(z)$, we eliminate the transverse dependence of Eq. (22) by multiplying its both sides by $\tilde{E}_{x0}^* = \sum_n e_{xn}^*\phi_n(y)\delta(s-j\beta_n)$, and integrating them over the waveguide cross section. The assumption of a slowly varying amplitude, $dA(z)/dz \ll \beta_n A(z)$, is transformed to s plane as $|\tilde{A}(s)| \gg |\tilde{A}(s-j\beta_n)|$ and $|s| \ll \beta_n$, for $n \neq 0$. Hence Eq. (22) is further simplified under this assumption to

$$s\tilde{A}(s) - A_0 = -\frac{1}{2c}\omega_{p0}^2\left[\sum_n (s-2j\beta_n)p_n\right]^{-1}\sum_m \frac{s-j\beta_m}{j(\omega-\omega_c)+(s-j\beta_m)\bar{V}_{0z}}F_{f_m}$$

$$\times \left\{\hat{Z}_m - \bar{\beta}_{ez} - \frac{1}{2}\bar{\beta}_{e\perp}^2\frac{j\omega\hat{Z}_m + (s-j\beta_m)c}{j(\omega-\omega_c)+(s-j\beta_m)\bar{V}_{0z}}\right\}p_m\tilde{A}(s), \tag{23}$$

where the effective cross section area and the em power flow of the nth harmonic are defined as

$$\Phi_n = \int_x\int_y \phi_n^2 dx\, dy, \tag{24a}$$

$$p_n = \Phi_n e_{xn}^* h_{yn}, \tag{24b}$$

respectively, and the corresponding electron beam filling factor is defined as

$$F_{f_n} = \Phi_n^{-1} \int_x \int_y g_0(x,y)\phi_n^2 dx\,dy. \tag{24c}$$

An interaction with the nth harmonic requires an operation in the vicinity of the cyclotron resonance $\omega - \omega_c - \beta_n \bar{V}_{0z} \sim 0$. Assuming that the various harmonic resonances are not coupled (i.e., that $|\omega - \omega_c - \beta_m \bar{V}_{0z}| \gg 0$ for any $m \neq n$), the dominant term in the sum over m in the right hand side of Eq. (23) is the nth term. Hence the dispersion relation of the periodic-waveguide cyclotron interaction is further simplified to

$$\tilde{A}(s) = \left\{ s[j(\omega - \omega_c) + (s - j\beta_n)V_{0z}]^2 + \frac{1}{2c}\omega_{p0}^2 F_{f_n} C_n(s) \left[[j(\omega - \omega_c) + (s - j\beta_n)\bar{V}_{0z}] \right.\right.$$

$$\left.\left. \times(\hat{Z}_n - \bar{\beta}_{ez}) - \frac{1}{2}\bar{\beta}_{e\perp}^2[j\omega\hat{Z}_n + (s - j\beta_n)c] \right] \right\}^{-1} [j(\omega - \omega_c) + (s - j\beta_m)V_{0z}]^2 A_0, \tag{25}$$

where $C_n(s)$ is defined as the nth harmonic power flow ratio,

$$C_n(s) = \frac{(s - j\beta_n)p_n}{\sum_m (s - 2j\beta_m)p_m}. \tag{26}$$

The dimensionless operating parameters of the periodic-waveguide cyclotron interaction are defined as follows. The tuning parameter for the nth harmonic is

$$\hat{\theta}_n = (\omega - \omega_c - \beta_n\bar{V}_{0z})\tau_0, \tag{27a}$$

where $\tau_0 = L/\bar{V}_{0z}$ is the electron time of flight along the interaction length L. The normalized space-charge parameter is

$$\hat{\theta}_p = \omega_p\tau_0, \tag{27b}$$

and the dimensionless wave number variables are defined as

$$\hat{s} = jsL, \tag{27c}$$

$$\hat{k} = kL, \tag{27d}$$

$$\hat{\beta}_n = \beta_n L. \tag{27e}$$

This notation leads to a simplified gain-dispersion relation as follows:

$$\tilde{A}(\hat{s}) = \frac{(\hat{s} - \hat{\theta}_n)^2}{\hat{s}(\hat{s} - \hat{\theta}_n)^2 - \frac{1}{2}\kappa_n(s)F_{f_n}C_n(s)\hat{\theta}_p^2}A_0, \tag{28}$$

where $\kappa_n(s)$, the complex coupling coefficient of the periodic-waveguide cyclotron interaction, is given by

$$\kappa_n(s) = \bar{\beta}_{ez}(\hat{s} - \hat{\theta}_n)(\hat{Z}_n - \bar{\beta}_{ez}) + \frac{1}{2}\bar{\beta}_{e\perp}^2(\hat{k}\hat{Z}_n - \hat{s} - \hat{\beta}_n). \tag{29}$$

The gain-dispersion equation in Eq. (28) resembles the Pierce equation which is valid in general for a wide range of traveling wave devices and free-electron lasers. The coupling term in Eq. (29), however, is more complicated and it incorporates different opposing effects, including the CRM and the Weibel effects. Each effect becomes dominant in the periodic-waveguide cyclotron operation in a different regime of the operating parameters $\hat{Z}_n$, $\bar{\beta}_{ez}$, and $\bar{\beta}_{e\perp}$. The general dispersion relation of the interaction (28) and (29) is analyzed in the following sections in various limits of the harmonic impedance for $\bar{\beta}_{e\perp} = 0$ and $\bar{\beta}_{e\perp} \neq 0$, and the physical interpretation of the various operating regimes is discussed.

III. ANALYSIS OF THE PERIODIC-WAVEGUIDE CYCLOTRON INTERACTION

In this section we analyze the gain-dispersion equation (28) at the fundamental harmonic ($n = 0$) in various operating regimes. In particular, we analyze the conditions for amplification in an on-axis injection of the electron beam into the periodic waveguide ($\bar{\beta}_{e\perp} = 0$). The periodic-waveguide cyclotron properties are discussed also for $\bar{\beta}_{e\perp} \neq 0$, in view of the known CRM and SWC types of interaction. In the following analysis we identify four different effects incorporated in the periodic-waveguide cyclotron interaction [these effects are indicated by e1–e4 in the following Eqs. (31) and (38)]. Each effect dominates in a different operating regime. Numerical solutions of Eq. (28) for parameters corresponding to ongoing experiments are presented in order to demonstrate the features of the periodic-waveguide cyclotron maser.

A. Zero initial transverse velocity ($\bar{\beta}_{e\perp} = 0$)

The gain-dispersion equation for a fundamental harmonic ($n = 0$) interaction with a zero initial transverse velocity ($\bar{\beta}_{e\perp} = 0$) results from Eqs. (28) and (29) as follows:

$$\tilde{A}(\hat{s}) = \frac{\hat{s} - \hat{\theta}_0}{\hat{s}(\hat{s} - \hat{\theta}_0) - \frac{1}{2}\bar{\beta}_{ez}(\hat{Z}_0 - \bar{\beta}_{ez})F_{f_0}C_0(\hat{s})\hat{\theta}_p^2}A_0. \tag{30}$$

In case that $\hat{\beta}_0 \gg \max|\hat{s}_i|$, where $\hat{s}_i$ denotes the poles of Eq. (28), we assume that the harmonic ratio $C_0(\hat{s})$ is weakly dependent on $\hat{s}$ and that it is dominated by the fundamental harmonic [i.e., $C_0(\hat{s}) \cong C_0(0) \sim 1/2$]. The response of the periodic-waveguide cyclotron depends then on the coupling parameter

$$Q_0 = \frac{1}{2}\bar{\beta}_{ez}(\overbrace{\hat{Z}_0}^{e1} - \overbrace{\bar{\beta}_{ez}}^{e2})F_{f_0}C_0(0)\hat{\theta}_p^2, \tag{31}$$

where e1 and e2 denote two opposing effects discussed later in this section. Using Eq. (31), the poles and the residues of Eq. (30) are given by

$$\hat{s}_{1,2} = \frac{1}{2}(\hat{\theta}_0 \pm \sqrt{\hat{\theta}_0^2 + 4Q_0}), \tag{32a}$$

$$r_{1,2} = 1 \pm \hat{\theta}_0/\sqrt{\hat{\theta}_0^2 + 4Q_0}, \tag{32b}$$

respectively, and the wave amplitude at $z = L$ results in the analytical expression

$$A(L) = A_0 \sum_{i=1}^{2} r_i e^{-j\hat{s}_i} = A_0 \left\{ \left(1 + \frac{\hat{\theta}_0}{\sqrt{\hat{\theta}_0^2 + 4Q_0}} \right) \exp\left[-\frac{j}{2}(\hat{\theta}_0 + \sqrt{\hat{\theta}_0^2 + 4Q_0}) \right] \right.$$
$$\left. + \left(1 - \frac{\hat{\theta}_0}{\sqrt{\hat{\theta}_0^2 + 4Q_0}} \right) \exp\left[-\frac{j}{2}(\hat{\theta}_0 - \sqrt{\hat{\theta}_0^2 + 4Q_0}) \right] \right\}. \tag{32c}$$

Equation (32c) has a different tendency for $Q_0 > 0$ and for $Q_0 < 0$. In a uniform waveguide, in which $\hat{Z}_0 \geq 1$ for the fundamental TE mode, the coupling parameter Q_0 (31) attains always positive real values. Thus the radiation power evolved along the interaction region is given by

$$|A(L)|^2 = A_0^2 \left[\cos^2\left(\frac{1}{2}\sqrt{\hat{\theta}_0^2 + 4Q_0} \right) \right.$$
$$\left. + \frac{\hat{\theta}_0^2}{\hat{\theta}_0^2 + 4Q_0} \sin^2\left(\frac{1}{2}\sqrt{\hat{\theta}_0^2 + 4Q_0} \right) \right], \tag{33}$$

which corresponds to a radiation absorption in the vicinity of the cyclotron resonance $\hat{\theta}_0 \sim 0$. The interaction is characterized in this case by radiation power loss rather than gain.

In an inductive periodic waveguide, the coupling parameter Q_0 may reach negative values or complex values [22]. For $Q_0 < 0$, Eq. (32c) yields a positive radiation gain. The coupling parameter Q_0 (31) becomes negative for a low harmonic impedance,

$$\hat{Z}_0 < \bar{\beta}_{ez}. \tag{34}$$

The fundamental harmonic impedance of the waveguide shown in Fig. 1 (as well as the periodic waveguide presented in Ref. [27]) is given in Eq. (A7) by $\hat{Z}_0 \cong \hat{\beta}_0 \hat{k}/\hat{k}_{10}^2$. Hence, the amplification condition of Eq. (34) is satisfied in the wave number range

$$\hat{\beta}_0 < \frac{\bar{\beta}_{ez} \hat{k}_{10}^2}{\hat{k}}. \tag{35}$$

In this operating regime, the periodic-waveguide cyclotron interaction may provide amplification even without initial electron transverse velocity component [as results from Eq. (32c) for $Q_0 < 0$]. The power growth for an optimal tuning ($\hat{\theta}_0 = 0$) is given by

$$|A(L)|^2 = A_0^2 \cosh^2(\sqrt{|Q_0|}), \tag{36}$$

which corresponds to an exponential growth along the interaction region.

A physical interpretation for the amplification condition in Eq. (35) is proposed on the basis of Poynting theorem. The integral

$$\frac{1}{2} \int_V \mathbf{E} \cdot \mathbf{J}^* dV \tag{37}$$

describes the radiation power evolved in a volume V due to a current source $\mathbf{J}$. In an ordinary cyclotron interaction, in the limit $\bar{\beta}_{e\perp} = 0$, the transverse force component in Eq. (9) is dominated by E_x, since $E_x > \bar{V}_{0z}\mu_0 H_y$.

Hence the radiation power is absorbed by the electron beam due to the transverse acceleration of the electrons by the radiation force as shown in Fig. 2. The coupling parameter Q_0 is dominated then by the term marked $e1$ in Eq. (31) which corresponds to the radiation absorption effect.

In an inductive periodic waveguide near cutoff, when the condition (35) is satisfied, the transverse force component in Eq. (9) is reversed (i.e., $E_x < \bar{V}_{0z}\mu_0 H_y$) and is dominated by the magnetic field component. Consequently, the corresponding term marked $e2$ is dominant in Eq. (31). The directions of the electron acceleration and the induced current are reversed in this case, and Eq. (37) may result then in radiation amplification rather than absorption. Energy is transferred in this process from the electron beam to the electromagnetic wave. The electron longitudinal velocity component is converted by the $\bar{V}_{0z}\mu_0 H_y$ magnetic force to a transverse velocity component as shown in Fig. 2. The transverse ac current induced in this mechanism appears in an opposite phase to the current induced by the electric field component, and consequently, Eq. (37) yields stimulated emission of radiation rather than absorption. The emission of radiation corresponds to the term $e2$ in Eq. (31)
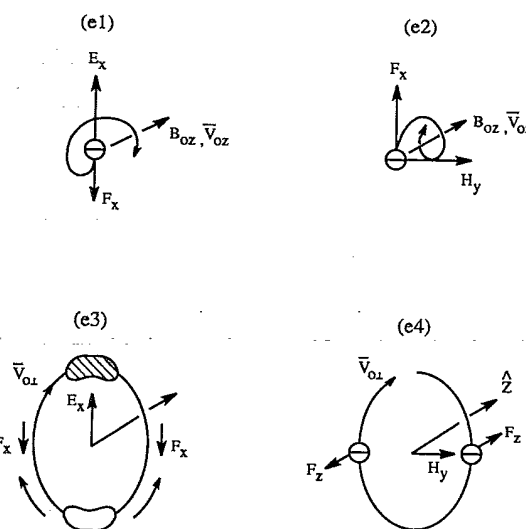

FIG. 2. Figurative descriptions of the four cyclotron effects incorporated in the periodic-waveguide cyclotron interaction: ($e1$) transverse electron acceleration by the electric field component; ($e2$) transverse electron acceleration by the magnetic field component (opposite to $e1$); ($e3$) relativistic azimuthal bunching due to the electric field component; ($e4$) axial bunching due to the magnetic field component.

TABLE I. Parameters for numerical examples.

			Example No. 1 Fig. 3:	Example No. 2 Figs. 4(a), 4(b), 4(c):
Electron beam energy	U_{eb}	[keV]	~ 8	~ 8
Electron beam current	I_{eb}	[A]	~ 0.75	~ 0.25
Rectangular tube	$a \times b$	[in.^{2}]	0.9×0.4	0.9×0.4
Metal post array:				
Periodicity	p	[mm]	20	20
Post diameter	t	[mm]	1.5	1.5
Post distance	d	[mm]	6.4	6.4
Length	L	[cm]	170	50
Frequency	$\omega/2\pi$	[GHz]	8.2	9.4
Solenoid field	B_{0z}	[kG]	2.95	3.07
Injection angle	$\bar{\beta}_{e\perp}/\bar{\beta}_{ez}$		0	0, 0.5, 1.0
Gain condition	Eq. (35)		satisfied	violated

and it dominates when the gain condition (35) is satisfied.

The analysis presented in this section provides an explanation for the mechanism of the interaction observed at M.I.T [22,23]. Its experimental parameters are listed as example 1 in Table I. No means are used in this amplifier experiment to spin up the electrons at the entrance to the interaction region. This periodic-waveguide cyclotron maser operates at $\sim$ 8.2 GHz. Thus, for $\hat{k} = 292$ m^{-1}, $\hat{k}_{10}$= 175 m^{-1}, and $\bar{\beta}_{ez}$=0.2, Eq. (35) results in $\hat{\beta}_0 < 20$ m^{-1} for a positive amplification. The result of Eq. (30) for the power gain ($|A(z)|^2/A_0^2$) in these conditions is shown in Fig. 3 as a function of the electron beam energy. This theoretical result, which shows gain without an initial transverse velocity, agrees well with the experimental observation reported in Refs. [22,23].

B. Nonzero initial transverse velocity ($\bar{\beta}_{e\perp} \neq 0$)

The evaluation of the periodic-waveguide cyclotron performance in the $\bar{\beta}_{e\perp} \neq 0$ operating regime requires a numerical solution of the third-order gain-dispersion equation (28) with the full complex coupling coefficient (29). Figure 4 demonstrates the effect of $\bar{\beta}_{e\perp} \neq 0$ for the parameters listed as example 2 in Table I. In this example the frequency and wave number are slightly higher
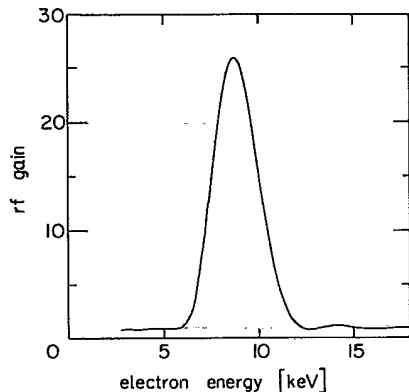

FIG. 3. Gain vs electron energy results from Eq. (30) for the parameters of example No. 1 in Table I with $\bar{\beta}_{e\perp}/\bar{\beta}_{ez} = 0$.

than that of the previous example and consequently the amplification condition (35) is violated. The result in Fig. 4(a) shows that for $\bar{\beta}_{e\perp} = 0$ the radiation is absorbed by the electron beam (as opposed to the previous example). The term marked $e1$ in Eq. (31) is dominant, hence the radiation power is spent near resonance on a transverse acceleration of the electrons in growing cyclotron trajectories. For $\bar{\beta}_{e\perp} > 0$, other effects dominate the periodic-waveguide cyclotron operation and it is reversed to an amplifier, as demonstrated in Figs. 4(b) and 4(c) for $\bar{\beta}_{e\perp}/\bar{\beta}_{ez} = 0.5$ and 1.0, respectively. The synchronism conditions for examples No. 1 and No. 2 are shown in Fig. 5.

The physical interpretation of the interaction in this regime corresponds to the known CRM and SWC interactions. The second term in the right hand side of Eq. (29),

$$\frac{1}{2}\bar{\beta}_{e\perp}^2 (\overbrace{\hat{k}\hat{Z}_0}^{e3} - \overbrace{\hat{s} - \hat{\beta}_0}^{e4}),\tag{38}$$

describes the coupling contributed by the initial transverse velocity of the electron beam. It consists of two terms illustrated in Fig. 2; the first term marked as $e3$ in Eq. (38) stems from the azimuthal bunching effect induced in the spiraling electron beam by the transverse electric field component E_x in the force equation (9). The energy transfer between the spiraling electrons and the em wave due to this component can be described by the known relativistic relation

$$\dot{\gamma} = -\frac{e}{mc^2}\mathbf{V}_{0\perp} \cdot \mathbf{E}_\perp.\tag{39}$$

Hence this interaction component ($e3$) corresponds to the known CRM-type relativistic azimuthal bunching effect as appears in the periodic waveguide cyclotron interaction.

The other interaction component marked as $e4$ in Eq. (38) stems from the $\mathbf{V}_{0\perp} \times \mathbf{H}_\perp$ axial bunching force. This component, referred to as *Weibel* interaction, opposes the effect of the CRM-type azimuthal bunching. In

the dielectric-loaded SWC interaction, this axial bunching force is the dominant effect [as results from Eq. (38) when $\hat{\beta}_0$ the normalized axial wave number is greater than the normalized waveguide impedance $\hat{k}\hat{Z}_0$]. In the periodic-waveguide cyclotron interaction, the CRM-type azimuthal bunching dominates the Weibel axial bunching for the fundamental harmonic operation ($n = 0$) when the impedance expression (A7) for the inductive periodic waveguide is valid.

The periodic-waveguide cyclotron interaction for $\bar{\beta}_{e\perp} \neq 0$ is dominated by an azimuthal CRM-type interaction rather than a longitudinal SWC-type interaction despite the resemblance of the *artificial-dielectric* peri-

odic waveguide to the SWC dielectric loaded waveguide. It should be noted, however, that the dielectric loaded SWC may also operate in a dominated azimuthal CRM-type interaction near cutoff as demonstrated clearly in Ref. [16]. A possible advantage of the periodic-waveguide cyclotron in this respect is that a near-cutoff operation in the fundamental mode is feasible in much higher frequencies than in an empty or a dielectric-loaded waveguide with the same dimensions.

C. Electron energy acceptance

The electron energy acceptance ($\Delta U = \Delta\gamma_0 mc^2$) for the periodic-waveguide cyclotron interaction can be estimated by Eq. (27a). The derivative of $\hat{\theta}_0$ by γ_0 yields

$$\frac{\Delta\gamma_0}{\gamma_0} = \frac{1}{\hat{k}_c}\frac{\gamma_{0z}^2 - 1}{\gamma_{0z}^2 - \omega/\omega_c}\Delta\hat{\theta}_0, \qquad (40)$$

where $\hat{k}_c = \omega_c L/\bar{V}_{0z}$, and $\gamma_{0z} = 1/\sqrt{1 - \bar{\beta}_{ex}^2}$. In the nonrelativistic limit ($\gamma_0 \cong \gamma_{0z} \cong 1$), the relative electron energy acceptance for $\bar{\beta}_{e\perp} = 0$ and $\gamma_{0z} \neq \sqrt{\omega/\omega_c}$) can be approximated by

$$\frac{\Delta U}{U_0} = \frac{\Delta\gamma_0}{\gamma_0 - 1} \cong \frac{2\Delta\hat{\theta}_0}{\hat{k}_c(\gamma_0^2 - \omega/\omega_c)}, \qquad (41)$$

where $U_0 = (\gamma_0 - 1)mc^2$ is the optimal electron kinetic energy for the periodic-waveguide cyclotron interaction. Assuming $\Delta\hat{\theta}_0 = 2\pi$, Eq. (41) yields $\Delta U/U_0 = 32\%$ for the parameters of example No. 1. The same result is obtained by Eq. (30) in Fig. 3, where ΔU (full width at half maximum)$\cong 2.8$ keV and $U_0 \cong 8.6$ keV. This theoretical estimate of the energy acceptance agrees well with the experimental result. In the amplifier experiment [22,23], the energy bandwidth of the measured gain curves is $\sim 1/3$ of the center energy.

The wide electron beam acceptance feature of the periodic-waveguide cyclotron interaction alleviates the electron beam quality requirements in terms of energy spread and energy variation. It may also result in a high-efficiency operation in the nonlinear regime.
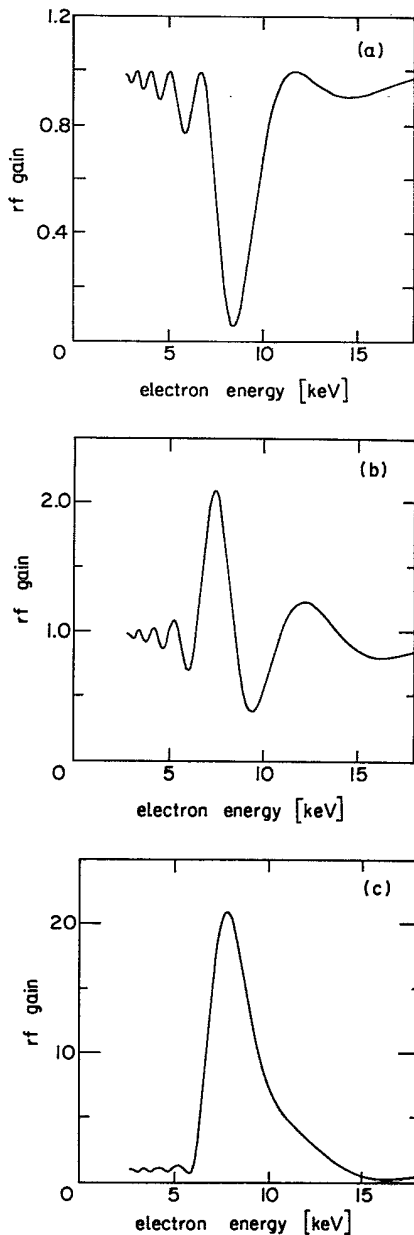

FIG. 4. Gain vs electron energy results from Eqs. (28) and (29) for the parameters of example No. 2 in Table I, with (a) $\bar{\beta}_{e\perp}/\bar{\beta}_{ex} = 0$, (b) $\bar{\beta}_{e\perp}/\bar{\beta}_{ex} = 0.5$, and (c) $\bar{\beta}_{e\perp}/\bar{\beta}_{ex} = 1.0$.
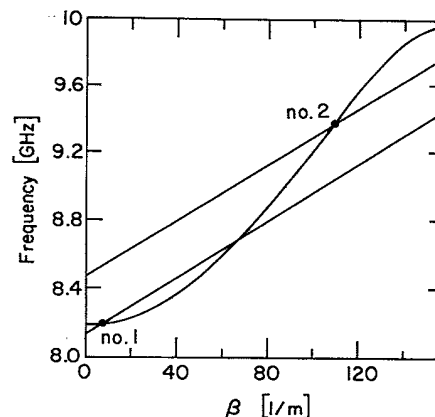

FIG. 5. Brillouin diagram of the inductive periodic waveguide and electron beam lines for examples No. 1 and No. 2.

IV. CONCLUSIONS

The theoretical model for the periodic waveguide cyclotron interaction presented in this paper confirms the recent experimental results presented in Refs. [22–25]. These studies show that the periodic-waveguide cyclotron interaction has the following interesting features.

(a) The coupling may occur at the cyclotron frequency near waveguide cutoff with a low-energy electron beam without an initial transverse velocity component.

(b) The acceptance of the interaction to electron energy variation is considerably wide. Both theory and experiment show an energy detuning ratio of $\Delta U/U_0 \sim 1/3$ for the parameters of example No. 1 in Table I.

(c) With a nonzero initial transverse velocity, the periodic-waveguide cyclotron interaction combines features of both CRM and SWC interactions. In the fundamental harmonic, however, it is dominated by the CRM azimuthal bunching effect.

(d) The use of a metallic periodic waveguide to slow down the wave alleviates technical difficulties typical to dielectric-loaded SWC devices.

Both experimental and theoretical studies indicate that the periodic-waveguide cyclotron concept may lead to the development of a compact source of microwave and millimeter radiation. The theoretical study presented in this paper provides a basis for further studies proposed as follows.

(a) Analysis of the waveguide dispersion and losses effect on the cyclotron interaction.

(b) Analysis of energy spread and angular spread effects.

(c) Extension of the present studies to other waveguide structures and in other frequency ranges.

(d) Analysis of the spontaneous emission of radiation and absolute cyclotron instabilities in periodic waveguides.

(e) A nonlinear analysis including a tapering of the metal-post array and/or the magnetic field.

(f) Analysis of backward-wave oscillations in the periodic-waveguide cyclotron oscillator experiment [24,25].

(g) Analysis of the interaction with high-order spatial harmonics.

Execution of these proposed studies may extend our understanding of the periodic-waveguide cyclotron interaction as a basis for a high-power, high-efficiency, and low-voltage source of microwave radiation.

ACKNOWLEDGMENTS

APPENDIX A: THE INDUCTIVE METAL-POST PERIODIC WAVEGUIDE

The impedance approximation of the periodic waveguide shown in Fig. 1 results from the following transmission line analysis. The dispersion relation of this periodic waveguide is given by [26] as

$$\cos(\beta_0 p) = \cos(k_{10}p) + \frac{1}{2}\bar{B}\sin(k_{10}p), \tag{A1}$$

where p is the period, $k_{10} = \sqrt{(\omega/c)^2 - (\pi/a)^2}$ is the wave number of the fundamental TE_{10} mode, and a is the waveguide width. The susceptance $\bar{B}$ of a symmetrical pair of posts is given approximately by

$$\bar{B} \cong 2\phi_{10}^2(d)\phi_{10}^2(t)\left[k_{10}\sum_{n=3,5,\dots}^{\infty}\frac{\phi_{n0}^2(d)\phi_{n0}^2(t)}{n^2\alpha_n}\right]^{-1}, \tag{A2}$$

where $\alpha_n = \sqrt{(n\pi/a)^2 - k^2}$ and $\phi_{n0}(x) = \sin(n\pi x/a)$ are the TE_{n0} mode decay rate and transverse profile, respectively, d is the distance between the post and the waveguide wall, and t is the radius of the metal post. Equation (A1) determines the dispersion relation $\omega(\beta)$ of the periodic waveguide shown in Fig. 1.

Using Floquet's theorem, the wave between two adjacent obstacles is described as

$E_x(0 \leq z \leq p)$

$$= e_{10}^+\phi_{10}e^{-jk_{10}z} + e_{10}^-\phi_{10}e^{jk_{10}z}$$
$$+ \sum_{n=3,5,\dots} e_{n0}\phi_{n0}(e^{-\alpha_n z} + e^{\alpha_n(z-p)}e^{-j\beta_0 p}). \tag{A3}$$

Hence the wave in each unit cell is composed of a forward (e_{10}^+) and a backward (e_{10}^-) components of the fundamental TE_{10} mode of the rectangular waveguide and of evanescent higher modes (e_{n0}) in the vicinity of the obstacles. The reflection coefficient for the TE_{10} mode for a given β_0 [as results from Eq. (A1)] is found to be

$$\Gamma_{10} = \frac{e_{10}^-}{e_{10}^+} = e^{-jk_{10}p}\frac{\sin[(k_{10} - \beta_0)p/2]}{\sin[(k_{10} + \beta_0)p/2]}, \tag{A4}$$

and the wave components of the zero harmonic in Eqs. (1a) and (1b) result in

$$e_{x0}\phi_0 = 4e_{10}^+\phi_{10}\frac{\beta_0}{\beta_0^2 - k_{10}^2}e^{j(\beta_0 - k_{10})p/2}$$
$$\times \sin[(\beta_0 - k_{10})p/2]$$
$$+ \sum_{m=3,5,\dots} e_{m0}\phi_{m0}\frac{2\alpha_m}{\beta_0^2 + \alpha_m^2} \tag{A5}$$

and

$$h_{y0}\phi_0 = \frac{2}{\omega\mu}\left(2e_{10}^+\phi_{10}\frac{k_{10}^2}{\beta_0^2 - k_{10}^2}e^{j(\beta_0 - k_{10})p/2}\right.$$
$$\times \sin[(\beta_0 - k_{10})p/2]$$
$$\left.+ \sum_{m=3,5,\dots} e_{m0}\phi_{m0}\frac{\beta_0}{\beta_0^2 + \alpha_m^2}\right). \tag{A6}$$

Each term is composed of two components, the first is contributed by the propagating fundamental mode, while the second ($\sum e_{m0}...$) introduces the evanescent higher modes effect. The latter is negligible in the transmission frequency bands of the waveguide, when $\hat{\beta}_0 \neq 0$. The wave impedance for the fundamental harmonic is determined then by the propagating mode and it results in

$$\hat{Z}_0 \cong \frac{\beta_0 k}{k_{10}^2}, \qquad\qquad\qquad (A7)$$

as in the slotted periodic waveguide presented in Ref. [27].

In the cutoff limit $\beta_0 \rightarrow 0$, the zero harmonic impedance is dominated by the evanescent modes and is given by

$$\hat{Z}_0(\beta_0 \rightarrow 0) \sim \frac{k}{2e_{10}^+\phi_{10}\sin(k_{10}p/2)}$$
$$\times \left(\sum_{m=3,5,...} \frac{e_{m0}\phi_{m0}}{\alpha_m} \right) e^{jk_{10}p/2}, \quad (A8)$$

which results in a complex number. The complex impedance in the cutoff limit corresponds to the stored em energy in the coupled-cavity structure in the transition frequency from transmission to cutoff (the impedance becomes pure imaginary in the stop band frequencies). The effect of a complex impedance on the periodic-waveguide cyclotron interaction is presented in Ref. [22].

[1] J. L. Hirshfield and J. M. Wachtel, Phys. Rev. Lett. **12**, 533 (1964).

[2] V. L. Bratman and A. E. Tokarev, Izv. Vyssh. Uchebn. Zaved. Radiofiz. **17**, 1224 (1974) [also in Radiophys. Quantum Electron. **17**, 932 (1974)].

[3] V. L. Bratman and M. A. Moiseev, Izv. Vyssh. Uchebn. Zaved. Radiofiz. **18**, 1045 (1975) [also in Radiophys. Quantum Electron. **18**, 772 (1975)].

[4] J. L. Hirshfield and V. L. Granatstein, IEEE Trans. Microwave Theory Tech. **25**, 522 (1977).

[5] K. R. Chu and J. L. Hirshfield, Phys. Fluids **21**, 461 (1978).

[6] V. L. Bratman, N. S. Ginzburg, G. S. Nusinovich, M. I. Petelin, and P. S. Strelkov, Int. J. Electron. **51**, 541 (1981).

[7] J. M. Baird, in *High Power Microwaves*, edited by V. L. Granatstein and I. Alexeff (Artech House, Boston, 1987).

[8] A. C. DiRienzo, G. Bekefi, C. Chen, and J. S. Wurtele, Phys. Fluids B **3**, 1755 (1991).

[9] A. Fruchtman and L. Friedland, IEEE J. Quantum Electron. QE-19, 327 (1983).

[10] A. W. Fliflet, Int. J. Electron. **61**, 1049 (1986).

[11] Shi-Chang Zhang, Phys. Fluids B **1**, 2502 (1990).

[12] R. Q. Twiss, Aust. J. Phys. **11**, 564 (1958).

[13] K. R. Chu, P. Sprangle, and V. L. Granatstein, Bull. Am. Phys. Soc. **23**, 748 (1978).

[14] J. M. Baird, S. Y. Park, K. R. Chu, H. Keren, and J. L. Hirshfield, Bull. Am. Phys. Soc. **25**, 911 (1980).

[15] K. R. Chu, A. K. Ganguly, V. L. Granatstein, J. L. Hirshfield, S. Y. Park, and J. M. Baird, Int. J. Electron. **51**, 493 (1981).

[16] H. Guo, L. Chen, H. Keren, and J. L. Hirshfield, Phys. Rev. Lett. **49**, 730 (1982).

[17] D. B. McDermott, H. B. Cao, and N. C. Luhmann, Int. J. Electron. **65**, 477 (1988).

[18] T. H. Kho and A. T. Lin, Phys. Rev. A **38**, 2883 (1988).

[19] H. B. Cao, D. B. McDermott, and N. C. Luhmann, *Initial operation of a Cherenkov CARM*, Proc. SPIE Vol. 1061 (SPIE Bellingham, WA, 1989), pp. 248–253.

[20] A. K. Ganguly and S. Ahn, Phys. Rev. A **42**, 3544 (1990).

[21] K. C. Leou, D. B. McDermott, and N. C. Luhmann, Jr., IEEE Trans. Plasma Sci. **20**, 188 (1992); and references therein.

[22] E. Jerby and G. Bekefi, *Nonrelativistic traveling wave cyclotron interaction*, Proc. SPIE Vol. 1872 (SPIE, Bellingham, WA, 1993), pp. 276–293.

[23] E. Jerby and G. Bekefi, Phys. Rev. E **48**, 4637 (1993).

[24] E. Jerby, G. Bekefi, A. Shahadi, E. Agmon, H. Golombek, V. Grinberg, and M. Bensal, *Backward-wave cyclotron maser oscillator experiment*, Proc. SPIE Vol. 2154 (SPIE, Bellingham, WA, in press).

[25] E. Jerby, G. Bekefi, and A. Shahadi, Nucl. Instrum. Methods Phys. Res. A **341**, 115 (1994).

[26] R. E. Collin, *Field Theory of Guided Waves* (McGraw-Hill, New York, 1960).

[27] E. Jerby, Phys. Rev. A **44**, 703 (1991).